A model-derived storm time asymmetric ring current driven electric field description

A. J. Ridley and M. W. Liemohn
University of Michigan, Ann Arbor, Michigan, USA

Received 21 February 2001; revised 6 August 2001; accepted 6 August 2001; published 1 August 2002.

[1] Low-latitude ionospheric and near-Earth magnetospheric electric fields are calculated from model results of the storm time asymmetric ring current. These fields are generated from subauroral field-aligned currents out of the ionosphere in the midnight sector and into the ionosphere on the dayside. The currents balance the divergence of the asymmetric ring current, which is the dominant component of the ring current during main phase and early recovery phase of magnetic storms. The basic shape of the electric potential pattern is described, both in the ionosphere and in the magnetosphere. It is found that intense ring current injection events can create potential differences up to 200 kV and can create local electric fields in the nightside magnetosphere >5 mV m^{-1}. The magnitudes and locations of the most intense electric fields are quite consistent with observations of subauroral (ionospheric) and near-Earth (magnetospheric) electric fields during magnetic storms. In addition, a relationship between the magnitude of the low-latitude electric potential and the *Dst** index is described. This relationship can be used to predict the location and size of strong low-latitude electric fields and currents. The presented electric field results are derived from model output, such that there is no feedback of the calculated fields back into the model. *INDEX TERMS:* 2730 Magnetospheric Physics: Magnetosphere—inner; 2712 Magnetospheric Physics: Electric fields (2411); 2409 Ionosphere: Current systems (2708); 2443 Ionosphere: Midlatitude ionosphere; *KEYWORDS:* inner magnetosphere, electric field, ring current, penetration electric field, polarization jet, currents

1. Introduction

[2] Penetration electric fields are those electric fields which are below the Region 2 current system. These fields can sometimes be very intense and can lead to phenomena such as ionospheric scintillation [*Kelley*, 1989] and plasmaspheric bite-outs [*Horwitz*, 1987]. Therefore it is important to understand not only their morphology and effects, but also their cause so that their occurrence and magnitude can be predicted.

[3] There are two electric fields that one might think of as being the penetration electric field: (1) the electric fields due to insufficient shielding by the Region 2 current system and (2) the electric field caused by the divergence of the asymmetric ring current. The first field is caused by rapid changes in the Region 1 field-aligned current patterns. When this current system increases substantially, there is not enough Region 2 current to shield it (since it increases at a much slower rate), and consequently the high-latitude electric potential pattern will stretch to much lower latitudes. On the other hand, when the Region 1 current system suddenly decreases, the Region 2 current system will be too large, and a reversed convection pattern may form until the Region 2 currents decrease to a level comparable to the Region 1 currents. The latter case is termed overshielding. This is the electric field most often associated with the term "penetration electric field." Extensive calculations have been made of this penetration field in the inner magnetosphere during disturbed conditions [*Southwood and Wolf*, 1978; *Spiro and Wolf*, 1984]. The impulsive Region 1 current changes are most pronounced during substorms. The penetration of this high-latitude potential pattern to lower latitudes during such events has been theoretically examined [*Spiro et al.*, 1988]. These results have even been used to explain equatorial electric field measurements from the Jicamarca incoherent scatter radar [*Fejer et al.*, 1990; *Fejer and Scherliess*, 1997]. While this field is most likely a ubiquitous source of penetration electric fields, it can only reach levels equivalent to the high-latitude (Region 1) electric fields, and therefore it is not capable of producing the large electric fields observed in the midlatitude ionosphere [e.g., *Foster et al.*, 1998] and the inner magnetosphere [e.g., *Wygant et al.*, 1998].

[4] There is reason to believe that the second source of penetration electric field (ring current driven) might actually dominate during storm events. The ring current has two components, an azimuthally symmetric ring of current generated by particles on closed drift trajectories and an azimuthally asymmetric crescent of current generated by the preferential drift of open-trajectory ions (the major carriers of energy) around the dusk side of the Earth. Therefore the asymmetric ring current is located in the dusk sector of the magnetosphere with a net westward total current. To close this current segment, an upward field-aligned current is formed in the ionosphere at low latitudes near midnight, and

Copyright 2002 by the American Geophysical Union.
0148-0227/02/2001JA000051$09.00

a downward current is formed at low latitudes on the dayside. The storm time asymmetry of the ring current has been observed by in situ and remote sensing instruments [*Burch et al.*, 2001a, 2001b, *Greenspan and Hamilton*, 2000] as well as modeled by various groups [*Takahashi et al.*, 1991; *Fok et al.*, 2001; *Liemohn et al.*, 2001b; *Ebihara and Ejiri*, 2000]. Recently, *Liemohn et al.* [2001a] calculated that the asymmetry component is dominant during the main and early recovery phases of geomagnetic storms, and *Cison Brandt et al.* [2000] showed that new energetic neutral atom imaging measurements confirm this result to be true for all storms observed by Imager for Magnetopause-to-Aurora Global Exploration (IMAGE) thus far. While the ionospheric currents produced by the divergence of the ring current are relatively weak ($\sim$2–5 times smaller than the Region 1 currents, or 0.5 μA m^{-2} during peak periods), they are essentially below the region of high conductivity (on the nightside), resulting in very strong electric fields. In addition, there are no current systems equatorward of this current, so the electric fields can extend to very low latitudes.

[5] Penetration (or low-latitude) electric fields typically occur during magnetic storms [*Burke et al.*, 1998; *Foster et al.*, 1998; *Foster and Rich*, 1998; *Yeh et al.*, 1991; *Wygant et al.*, 1998; *Rowland and Wygant*, 1998; *Reddy and Mayr*, 1998] when the energy input into the magnetosphere and ionosphere are intense and the ring current is strongest. They also occur most often in the dusk and evening sectors. While there are numerous observations of these fields, a quantitative observation of their global structure is presently quite difficult. For instance, Defense Meteorological Satellite Program (DMSP) satellite observations have recorded penetration electric fields of up to 70 kV [*Burke et al.*, 1998], while *Reddy and Mayr* [1998] showed DE 2 measurements of 800 m s^{-1} flows at low latitudes, but there are severe limitations to these types of measurements. Each DMSP satellite (or the DE 2 satellite) is confined to a magnetic local time (MLT) band which only allows for a measurement of this field within a small area (i.e., along the satellite track). This area may be quite distant from the most intense electric fields. In addition, the orbital period of the satellites is $\sim$100 min, which means that the satellite may miss the most intense time periods. The spatial and temporal limitations of the satellites implies that the inferred electric fields are most likely a lower bounds on the actual electric fields which may exist at any time during the storm period. This limitation is true of any satellite measurements of the penetration electric field.

[6] The suite of incoherent and coherent scatter radars has the ability to measure a significant portion of the high-latitude ionospheric flow pattern [e.g., *Ruohoniemi and Greenwald*, 1996]. Most of these radars, however, are pointed poleward. The Millstone Hill incoherent scatter radar is one of the only radars that has been used to sample the latitudes in which the penetration electric fields manifest. There have been numerous studies which have resulted from observations taken from this radar [e.g., *Foster et al.*, 1998; *Foster and Rich*, 1998; *Yeh et al.*, 1991]. Ionospheric plasma flows exceeding 1000 m s^{-1} have been observed, indicating the presence of large eastward and/or poleward electric fields in the evening sector at midlatitudes. Again, these large drift speeds were observed during the main phase of magnetic storms. While these studies do a good job of describing the basic features of the penetration electric field, they could not describe the global characteristics of the field. This is true for other incoherent scatter radars such as Jicamarca [e.g., *Fejer et al.*, 1990; *Fejer and Scherliess*, 1997].

[7] Satellite measurements of penetration electric fields have also been made in the inner magnetosphere, particularly with the CRRES satellite [*Burke et al.*, 1998; *Wygant et al.*, 1998; *Rowland and Wygant*, 1998]. *Rowland and Wygant* [1998] compiled a mission-long (noon around dusk to 0400 LT) statistical profile of the observed electric field with radial distance and activity level (Kp), discovering that the E_y (GSE coordinates) component of the field reverses from the standard Volland-Stern [*Volland*, 1973; *Stern*, 1975] shielded field profile and actually grows with decreasing radial distance. In fact, the magnitude is suppressed (relative to a shielded Volland-Stern) beyond $\sim$6 R_E and is enhanced inside of this. This suppression at larger radial distances is an interesting feature that will be examined in section 3. In addition to the statistical model, *Wygant et al.* [1998] found penetration fields exceeding 6 mV m^{-1} inside of 4 R_E during the ring current injection intervals of a large magnetic storm.

[8] While we have been using the term penetration electric field for sources of electric fields both at low latitudes and in the near-Earth magnetosphere, we would like to make a distinction between them. For this study, we refer to the electric field associated with the ring current as being the asymmetric ring current driven electric field, while the observations of low-latitude electric fields are referred to as penetration electric fields. Low-latitude electric fields caused by undershielding are not considered in this study.

[9] So, the question remains: What is the magnitude and morphology of the global storm time low-latitude (ionospheric) and near-Earth (magnetospheric) electric field driven by the asymmetric ring current? There currently exists no data analysis methodology for examining the high time resolution global characteristics of this electric field. *Burch et al.* [2001a] showed dynamics of the plamasphere during a magnetic storm. From this type of analysis it may be possible to determine the instantaneous electric field in the inner magnetosphere, although this technique has not been used as of yet. We are therefore forced to examine model results to describe its global, time-dependent behavior. Observations can then be used to validate and enhance this description. This study describes the spatial and temporal characteristics of the storm time asymmetric ring current driven electric field found by determining the closure currents from results of a ring current model for a number of magnetic storms. Because the ring current results are not calculated self-consistently with the electric field, the results presented in section 3 are most likely an upper limit on the magnitude of the electric field.

2. Technique

[10] This study describes the electric fields modeled by the Michigan Ring Current-Atmosphere Interaction Model

(RAM) [*Fok*, 1993; *Jordanova et al.*, 1996; *Liemohn et al.*, 2001b]. The program solves the time-dependent, gyration- and bounce-averaged kinetic equation for the phase-space distribution function of a chosen ring current species. The five independent variables are time, geocentric distance in the equatorial plane, magnetic local time, kinetic energy, and equatorial pitch angle. The solution of the kinetic equation is accomplished by replacing the derivatives with second-order accurate, finite volume, numerical operators. The source term for the distribution function is the outer simulation boundary, where observed particle fluxes from geosynchronous orbiting satellites (such as those maintained by Los Alamos National Laboratory (LANL)) are applied as input functions. Because the multiple-particle analyzer (MPA) [*McComas et al.*, 1993] and Senior Officer Present Afloat (SOPA) [*Belian et al.*, 1992] instruments on the LANL satellites do not resolve ion mass, the composition of the incoming particles is determined from the statistical relationships derived by *Young et al.* [1982] from previous geosynchronous orbit measurements. This plasma is then convected through the simulation region by the convection electric field (defined by *McIlwain* [1986] and *Liemohn et al.* [2001b]), magnetic gradient-curvature drifts, and corotation effects. Other processes included in the calculation are Coulomb collisions, charge exchange, and atmospheric precipitation.

[11] This code was recently modified to calculate the field-aligned current due to the divergence of the cross-field current within the simulation region [*Liemohn et al.*, 2001a]. These field-aligned currents are then mapped to ionospheric altitudes to determine how the currents close in the ionosphere. This procedure was developed to analyze the effect of the closure currents on the measurements of *Dst* by low- and middle-latitude magnetometer stations. However, they can also be used to investigate the electric potential generated by these field-aligned currents.

[12] In order to accurately determine the closure currents of any current system, the ionospheric electric field must first be solved for. This is done through the equation

$$j_R(R_E) = [\nabla_\perp \cdot (\Sigma \cdot \nabla\psi)_\perp]_{R=R_E}, \quad (1)$$

which describes the relationship between the height-integrated conductance tensor, Σ, the ionospheric potential, ψ, and the radial component of the current, j_R. The closure currents are then described by the equation

$$j_\perp(R_E) = \Sigma \cdot \nabla\psi. \quad (2)$$

[13] In this study, the electric potential pattern derived from (1) is examined. This pattern is what is termed the storm time asymmetric ring current driven electric potential, while the electric field is derived by taking the gradient of the potential.

[14] To derive the electric potential, a conductance pattern needs to be known. The ionospheric conductance typically has a number of components, such as solar illumination, starlight, auroral particle precipitation, and precipitation within the polar cap [see, e.g., *Roble and Ridley*, 1987]. The solar illumination conductance was derived using the model by *Moen and Brekke* [1993]. The starlight and polar cap conductance components were held constant at 0.5 mhos each. The auroral precipitation conductance was derived using an empirical relationship between the field aligned current specified by the ring current model and the conductances. This auroral precipitation model is further described by A. J. Ridley (An ionospheric conductance model based upon field-aligned currents, manuscript in preparation, 2002).

[15] There are a number of uses for the derived low-latitude electric potential pattern. For example, the potential can be superposed onto a high-latitude pattern which excludes the storm time, low-latitude electric field, such as models by *Weimer* [1996], *Ridley et al.* [2000], etc. This total electric field can either be used to study the thermosphere-ionosphere system or it can be mapped along field lines and used to produce equipotentials in the magnetosphere for use in ring current modeling. The use of the near-Earth electric field in the ring current model would make it a self-consistent calculation and may have the effect of altering the entire ring current structure. However, such a feedback is beyond the scope of the present study, and the field-aligned currents used in this study were derived through post-processing of results from the model as described above.

3. Results

[16] The ring current model was run for four magnetic storms: 6–9 June 1991, 14–17 May 1997, 24–27 September 1998, and 18–21 October 1998. The results for these storms are described in detail by *Liemohn et al.* [2001a, 2001b] and *Kozyra et al.* [2001]. In summary, Figure 1 shows the observed and calculated *Dst** profiles for these events. It was shown that most of the energy content of the ring current during the main and early recovery phases of all of these storms is carried by ions on open drift trajectories (that is, particles making only a single pass through the inner magnetosphere) [*Liemohn et al.*, 2001b]. The resulting current system is then highly asymmetric, and this partial current loop must be closed somehow. Calculating the divergence of the perpendicular currents in the magnetosphere yields the field-aligned currents necessary for closure. It was shown by *Liemohn et al.* [2001a] that at least 75% of the asymmetric current system closes in this manner. The field-aligned currents flow into (or out of) the ionosphere, requiring horizontal currents in the ionosphere for complete closure of the current loop. This ionospheric current system generates an electric field (according to Ohm's law). Because there is no oppositely signed field-aligned current equatorward of this system, the influence of these electric fields spreads to very low latitudes, generating the low-latitude (or penetration) electric field.

[17] Hourly field-aligned current patterns were derived from these results and were subsequently used to determine the electric potential for each period. Figure 2 shows the model results for five time periods during the September 1998 storm. During the prestorm and injection times (the top two rows in Figure 2) the potential minimum was located at $\sim 60^\circ$ latitude and 0000 MLT. At the peak of the storm (the middle row in Figure 2) the minimum in

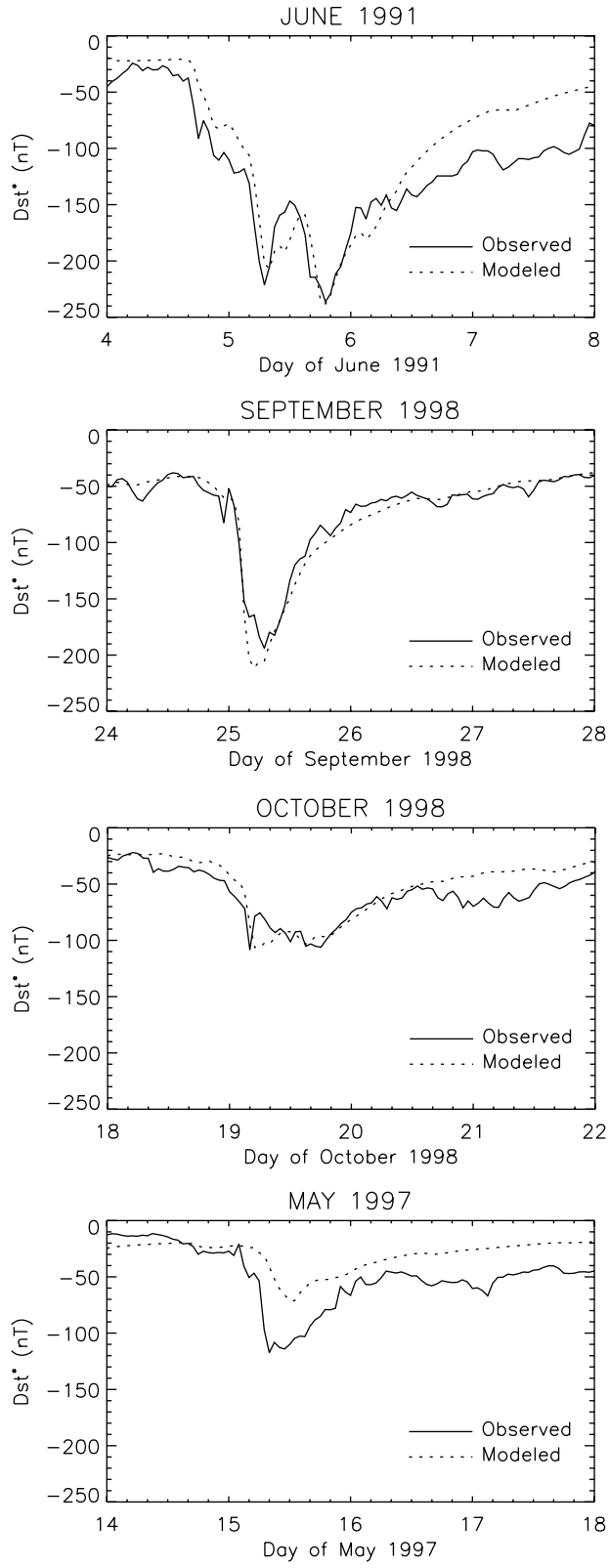

Figure 1. Time profiles of the observed and modeled *Dst** values for the four storms to be examined in this study.

potential rotates around to ~2200 MLT and moves to slightly lower latitudes. By the recovery phase the minimum rotates a bit farther toward dusk, but not significantly, with most of the change occurring in the intensity of the potential well.

[18] The maximum in potential is much weaker than the minimum for two reasons. The first is that the field-aligned current on the dayside is spread out over a much wider MLT sector and is therefore weaker at each location. The second is that the conductance on the dayside is much stronger and more uniform, allowing a smaller electric field to drive similar magnitude currents. The maximum also tends to rotate much farther than the minimum in potential. This is due not only to the electric field model in the magnetosphere [*McIlwain*, 1986; *Liemohn et al.*, 2001b] but also to the dayside conductance damping the potential around noon.

[19] Subtracting the minimum potential value from the maximum potential value yields a convenient quantity that characterizes the strength of the low-latitude electric field, the cross-polar cap potential (CPCP). Figure 3 shows this value for the four storms of interest. It is seen that the peak values of the CPCP can reach 200 kV (even 250 kV at one time during the September 1998 storm). Note that this CPCP is a different value than the CPCP for the Region 1 currents and is in fact comparable to (and even greater than) the Region 1 CPCP, seen in Figure 4. However, the low-latitude CPCP is spatially removed from the Region 1 potential structure, and so the total CPCP will not be much larger than the maximum of these two values. Comparing Figure 3 with Figure 1, it is seen that the peak low-latitude CPCP always occurs just prior to the storm peak. This is because the field is created by the asymmetry in the ring current, which peaks at this time as well [*Liemohn et al.*, 2001a]. At the actual *Dst** minimum the inflow and outflow of ring current energy balance, which occurs after the time of the maximum injection rate of hot ions into the inner magnetosphere. Another interesting feature of Figure 3 is that the maxima in CPCP are not necessarily correlated to the depth of the corresponding *Dst** minimum. It is actually the rate of ring current injection that governs the size of the CPCP. This correlation will be discussed in more detail in section 4.

[20] If we assume that the magnetic field lines of the inner magnetosphere are equipotentials, then the electric potential values in the ionosphere can be mapped out into the magnetosphere. Figure 5 shows the storm time asymmetric ring current driven potential and the corresponding electric field components in the equatorial plane of the magnetosphere. The rows are at the same times during the September 1998 storm as those shown in Figure 2. The mapping was done with the same assumption used in the earlier mapping of the field-aligned currents (and in the ring current model calculations): that the magnetic field is a dipole. This mapping has the effect of compressing the potential structure at small radial distances while expanding it at large radial distances. This is seen clearly in the electric field components (the spatial derivative of the potential), as the largest fields are inside of 3 R_E. The electric fields are directed from high to low potential, so there is a strong radially outward electric field near midnight near the Earth and strong azimuthal electric fields in the post-dusk and

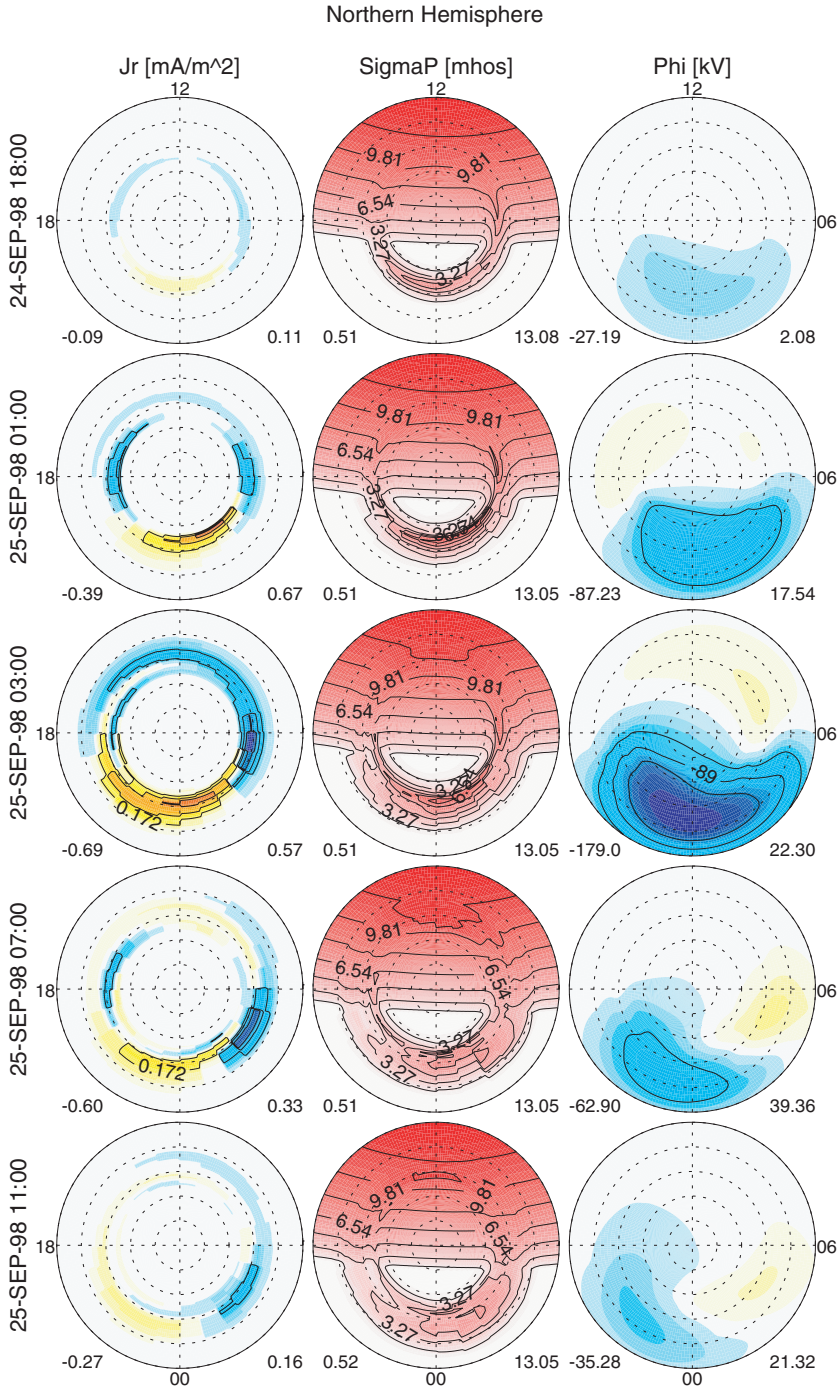

Figure 2. Ionospheric quantities at five times during the September 1998 magnetic storm. The left-hand column is the radial current density into (blue) and out of (yellow) the ionosphere calculated from the ring current model results (in $\mu A/m^2$), the middle column is the height-integrated conductance (in mhos), and the right-hand column is the derived potential pattern showing negative (blue) and positive (yellow) potential structures (in kV). Given below each subplot are the minimum and maximum quantities for that plot. The five times chosen are before the main injection, during the initial storm growth, just before the *Dst** minimum, in the early recovery, and near the transition from fast to slow recovery timescales. Dotted-line contours are spaced every 10° magnetic latitude, with noon at the top and dawn to the right in each subplot.

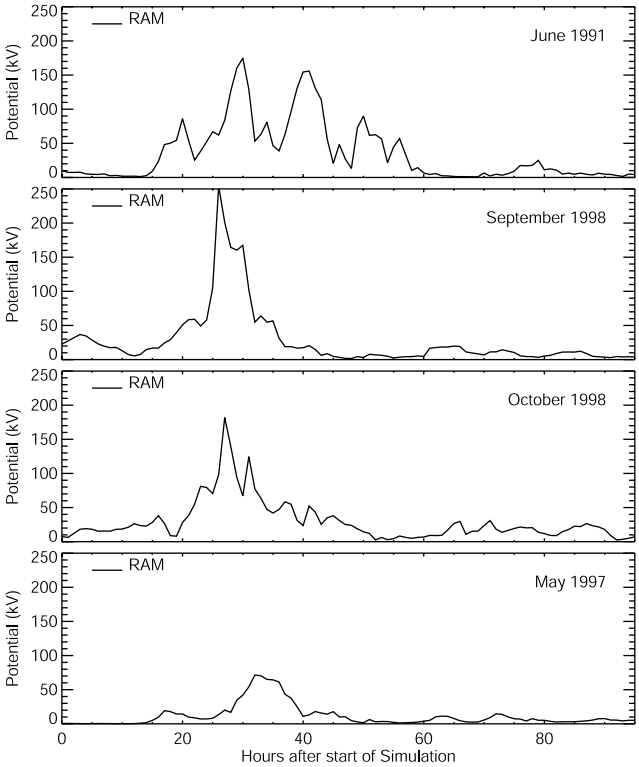

Figure 3. Cross-polar cap potential (CPCP) difference from the penetration field calculations for the four storms of interest.

predawn sectors. At the time of the CPCP peak, the electric field reaches 10 mV m^{-1} inside of 3 R_E.

4. Discussion

[21] Although the description in section 3 is interesting, it is meaningless unless it is shown to be consistent with observations. We therefore examine the description of the storm time asymmetric ring current driven electric fields in comparison with published observations of penetration electric fields. Note that the storms which have been investigated in the literature are not necessarily the same storms which were modeled here. Therefore only general features can be examined, such as location and magnitude of the strongest electric field.

[22] The papers by *Foster et al.* [1998] and *Foster and Rich* [1998] describe Millstone Hill and DMSP observations of penetration electric fields during the March 1990 and November 1993 storms. The March 1990 storm contained large flow velocities between 1900 and 2100 MLT at low latitudes (35°) and midlatitudes (52°), while the November 1993 storm showed strong flows between 59° and 66°. The modeled electric field is consistent with the strong midlatitude flows. The exact location of the peak flows is highly dependent upon the trajectory of the DMSP satellite, which was not published, but the approximate location is consistent with the model. The low-latitude electric field was not represented within the model.

[23] Comparisons with equatorial electric field measurements, such as those of *Fejer et al.* [1990], are not possible because of the boundary conditions used in the present study (ϕ = 0 at 35°). *Fejer and Scherliess* [1997, 1998] make a convincing case that there is a relationship between the hot plasma dynamics of the inner magnetosphere and the electric fields at the equator. However, this is most likely the penetration of the high-latitude potential pattern due to undershielding of the substorm current system (the undershielded electric field, as discussed above), as the model results used in these studies for the magnetospheric ion flows did not create a deep injection of plasma capable of producing a ring current type of penetration field, as is being discussed here. Therefore those results and the results presented here are complementary. It should be noted, though, that the penetration of the electric fields generated by Region 1 currents down to the equator means that the boundary condition used in the present study is most likely too severe. However, such a modification will not alter the main conclusions of this study, which are that the asymmetric ring current can generate intense electric fields in the subauroral ionosphere and magnetosphere and that a relationship exists between the total potential difference of this field and *Dst**.

[24] The present model actually includes the Region 2 currents lying within the simulation domain of RAM (geosynchronous orbit). This is not clearly seen in Figures 2 and 5 because of the color scales used and the UTs chosen for presentation, but *Liemohn et al.* [2001a] discuss this in more detail. It was shown there that the model reproduces the inner edge of this field-aligned current system and that the calculated current densities are quite similar to those observed in near-Earth space.

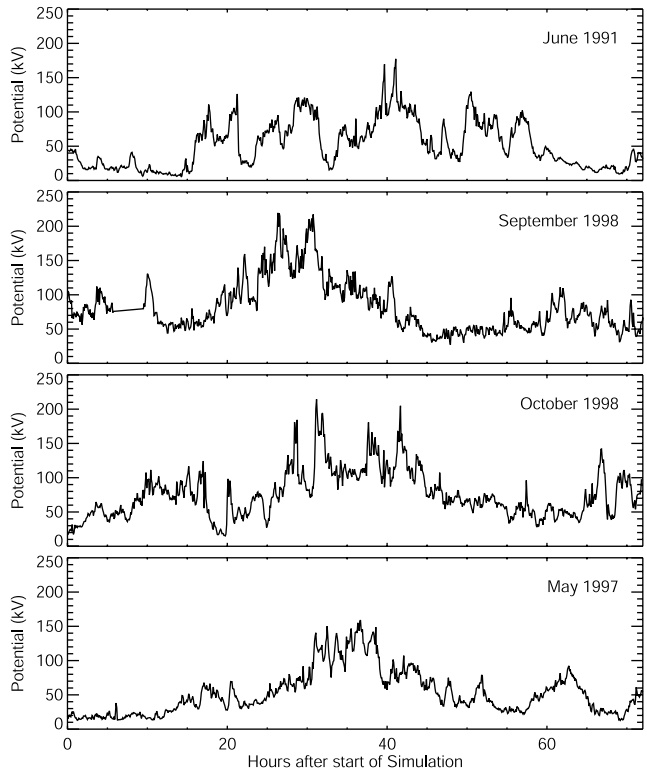

Figure 4. CPCP difference from the high-latitude current system as found by the assimilated mapping of ionospheric electrodynamics (AMIE) technique [c.f. *Liemohn et al.*, 2001b and *Kozyra et al.*, 2001].

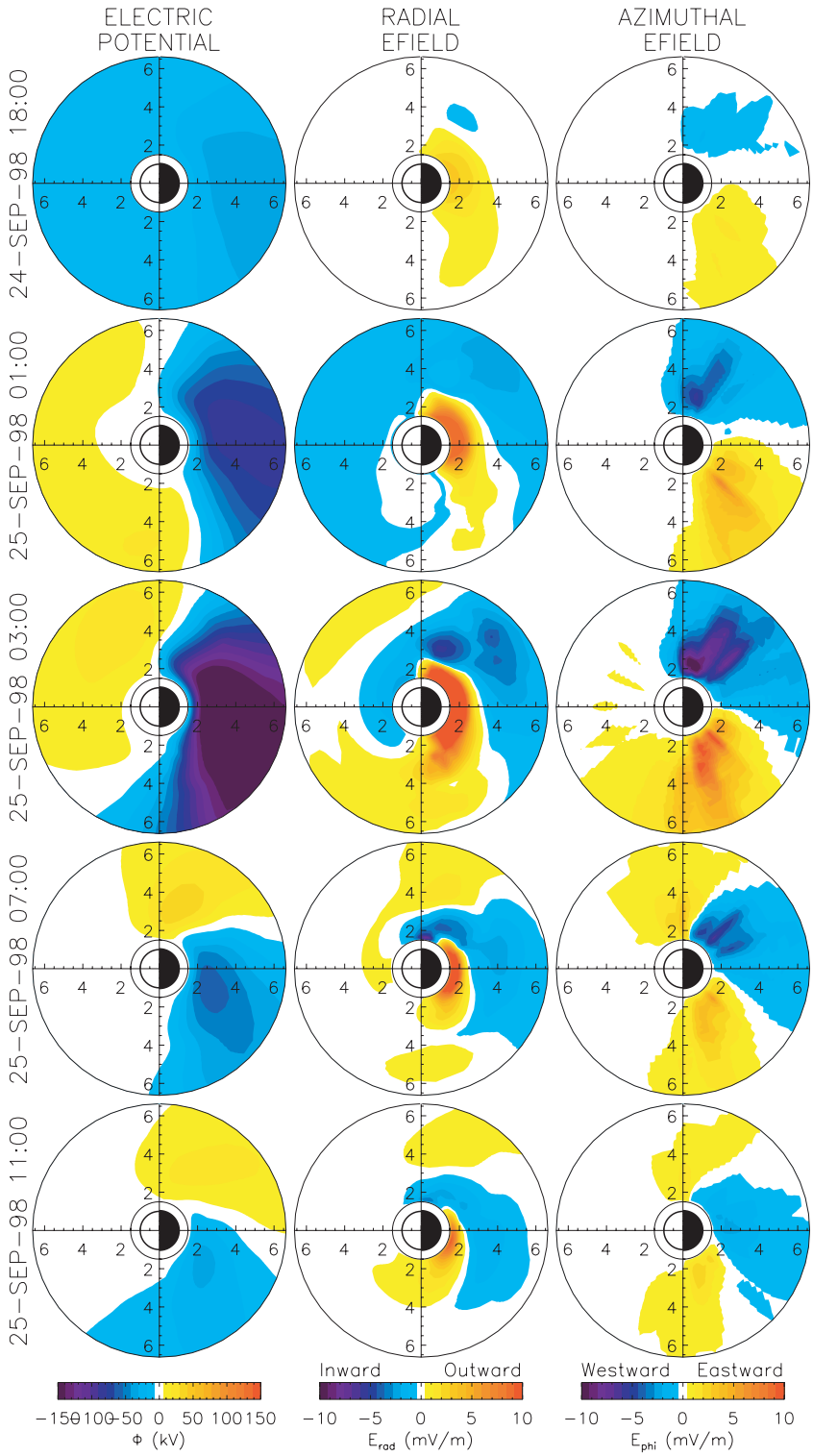

Figure 5. Penetration field quantities mapped out along dipole field lines to the equatorial plane of the magnetosphere for the five times given in Figure 2. The left-hand column is the potential and the middle and right-hand columns are the radial and azimuthal components of the electric field. Axis values are in R_E, with the sun to the left and dawn to the top in each subplot. Below each column is the corresponding color scale.

[25] At the peak of the storms, outward electric fields in the inner magnetosphere just after dusk reach 10 mV m^{-1} (see Figure 5). These are larger than those observed by CRRES [*Wygant et al.*, 1998] for an even larger magnetic storm (that of March 1991). However, the largest fields occur inside of L = 2 where the noise in the CRRES electric field data becomes large and the results become suspect. Outside of L = 2 the largest modeled electric field in the

duskward direction was 7 mV m^{-1}, which is much more consistent with the CRRES observations.

[26] The L-shell and activity-dependent profiles of the electric field near dusk are also consistent with the CRRES observations compiled by *Rowland and Wygant* [1998]. At low activity the ring current induced near-Earth electric field is negligible. However, at high activity it can be larger than the main convection field. Beyond geosynchronous orbit the model results show that the main dawn-to-dusk electric field is completely damped by the ring current induced penetration electric field, while inside of this radial distance the main convection field is enhanced. This is exactly the trend seen in the *Rowland and Wygant* [1998] statistics. Note, however, that the binning of the data in that compilation blurs the true magnitude of the near-Earth electric field for any particular event, which can be far more intense for short time periods than the average field for that activity level.

[27] Finally, comparison with the DMSP data of *Burke et al.* [1998] shows that satellite passes near dusk may actually miss the bulk of the low-latitude electric field. During the intense injection events of this storm (June 1991, which was modeled), the peak of the field-aligned closure currents is found to be near midnight in the ring current model results. The negative potential structure on the nightside weakens with decreasing local time. It is possible that the satellites, which only recorded a peak low-latitude potential of 70 kV, did not sample the spatial location of the peak modeled potential. Because of the short durations of the intense maxima in the (modeled) low-latitude electric field, it is also possible that the DMSP satellites did not sample the temporal location of the peak.

[28] These inner magnetospheric electric fields will certainly have an impact on the plasma in the region, both the thermal core of the plasmasphere and the hot plasma of the ring current. For instance, the observations from the IMAGE satellite show that the nightside plasmasphere can be highly structured during magnetic storms, with the appearance of shoulders, bite-outs, and tails [e.g., *Burch et al.*, 2001a, 2001b]. All of these could be explained in light of the morphology of the near-Earth electric field generated by the asymmetric ring current. Because these electric fields can be equal to or larger than the corotation field at these locations, the thermal plasma's eastward drift can be momentarily slowed, stopped, or even reversed. Such a change in flow can create the features seen in the storm time data from IMAGE.

[29] The hot plasma will also be effected by the near-Earth electric field. However, because the plasma has been adiabatically energized by the time it reaches the locations of the largest fields, the westward gradient-curvature drift is quite large. Therefore these fields will most likely not cause a drastic redistribution of the ring current particles. Inside of the potential minimum, however, the near-Earth field induces a drift that complements the gradient-curvature drift. Thus these particles will more rapidly convect through the inner magnetosphere. Such an influence will increase the percentage of ion energy being carried by particles on open drift paths. In addition, it will probably decrease the magnitude and duration of the strong near-Earth electric field. Therefore it is expected that when the electric field is calculated self-consistently within the model, the magnitude of the derived electric field will be weakened, and the pattern will probably stretch (with the maximum possibly rotating) toward dusk. While these speculations may be valid, the processes are complex enough that the results will not be known until an actual self-consistent run is carried out.

[30] It should be noted that this is not the first study to theoretically calculate the size of the storm time near-Earth electric field. In particular, the Rice Convection Model (RCM) has included it in its calculation scheme from its creation [e.g., *Harel et al.*, 1981]. Examination of this and other more recent RCM studies [e.g., *Garner*, 2000; *Fok et al.*, 2001] show a "tongue" in the electric potential contours from midnight toward dawn in the inner magnetosphere. This is very similar to the morphology of the model results described above. That is, the electric potential contours in Figure 5, when superposed with the magnetospheric convection electric potential pattern, yields a pattern with a predominantly sunward flow with the exception of a dawnward distortion on the nightside inside of geosynchronous orbit. However, the magnitude of the RCM-generated near-Earth field is, in general, smaller than that found here.

[31] There are a number of possibilities for why the magnitudes may differ: (1) the electric field is highly dependent upon the ionospheric conductance which is used (a lower conductance causes a higher electric field), so the RCM may have higher conductance than the model presented here; (2) the currents within the RCM and the RAM codes are calculated differently, such that the RAM code may always have higher currents than the RCM; (3) the RCM has a self-consistent electric field, while the electric fields which are presented above are all derived through post-processing the model results; and (4) the RCM does not include all of the proper scattering and loss terms, nor do they resolve the velocity space distribution with nearly the level of accuracy attained with the RAM. Therefore, while neither model is a comprehensive calculation of the storm time asymmetric ring current driven electric field, each produces a seemingly acceptable description. Determination of the true electric field will have to wait for additional model development and for comparisons with data. This true electric field pattern is most likely somewhere in between those presented here and those generated by the RCM, results that are already qualitatively very similar.

5. Applicability to Space Weather

[32] The description in section 4 of the low-latitude storm time electric fields can be summarized into a normalized potential pattern and a relation between the *Dst** index and the CPCP of the potential pattern. This simplified description of the model results is useful for space weather applications. Namely, the description can be keyed off of a real-time *Dst** specification (or prediction) to describe the current (or future) ionospheric and magnetospheric electric field patterns at low latitude and low L-shell values, respectively.

5.1. Limitations of Existing Models

[33] Currently, there are a number of models which predict the electric potential pattern in real time [e.g., *Ruohoniemi and Greenwald*, 1996; *Ridley et al.*, 2000].

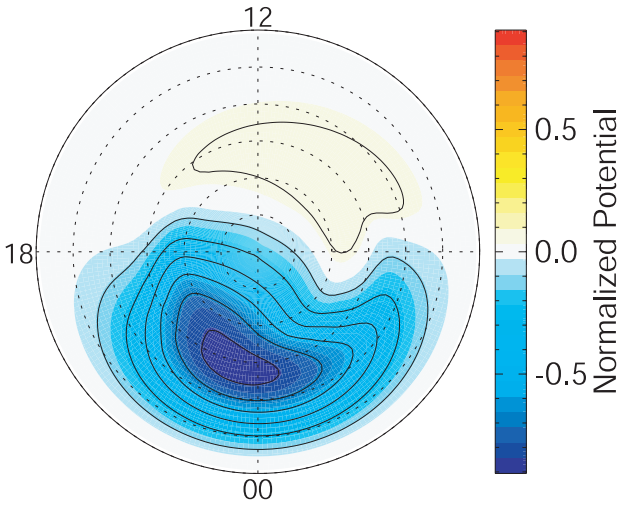

Figure 6. Average morphology of the penetration electric potential in the ionosphere.

None of these techniques allows for the prediction of low-latitude electric fields, which may in fact cause the largest space weather effects. We discuss the limitations of the real-time assimilated mapping of ionospheric electrodynamics (AMIE) technique here and describe how the relationships shown here could improve the specification ability of the technique.

[34] The AMIE technique was originally designed for examining auroral zone and polar cap phenomena. In the high-latitude region a number of assumptions can be made which simplify the technique, such as the magnetic field lines being vertical. At lower latitudes this assumption breaks down, and a much more rigorous approach is needed. In addition, the boundary conditions within the AMIE technique are such that the electric potential at the lowest latitude must be sloped toward zero. These two conditions make modeling disturbed time periods very difficult.

[35] For example, when a magnetic storm is occurring, the auroral oval could expand down to 55° magnetic latitude or lower. In this region the dipole tilt is ~35°, which makes the vertical field line approximation invalid. In addition, the lower boundary of AMIE is within 10° of this location, so very strong fields can be damped by the boundary condition.

[36] The vertical field line assumption enters through the relationship between the ionospheric conductance, ground magnetic perturbations, and the electric potential. If an AMIE run were conducted solely using electric field measurements, these lower latitude electric fields would be much more accurately modeled. There is a tendency, though, for electric field measurements to be concentrated at higher latitudes. For example, most of the Super Dual Auroral Radar Network (SuperDARN) radars take measurements throughout the auroral zone and into the polar cap, while few take measurements equatorward of the auroral zone. In addition, the DMSP satellites that are capable of measuring accurate electric fields in this region [e.g., *Burke et al.*, 1998], although they do so for a very limited time, so an accurate high time resolution evolution of these strong electric fields cannot be determined.

[37] The use of a simplified description of the low-latitude storm time electric fields would allow one to not have to change the basic electric field model, such as real-time AMIE. The derived electric fields could simply be added on to the AMIE (or *Weimer* [1996], *Papitashvili et al.* [1999], *Ruohoniemi and Greenwald* [1996], etc.) derived patterns. This technique allows one to model the large electric fields at low latitudes without significant modification to the basic code and brings the modeled electric fields much more in line with the observed fields.

5.2. Low-Latitude Electric Field Prediction Algorithm

[38] Using the output from the four modeled time periods described in section 3, general shape of the low-latitude storm time electric field pattern was generated, and it's relationship to *Dst** was examined. Because the general shape of the pattern remained approximately the same throughout the intervals, all of the patterns were averaged together and normalized to give the basic shape of the potential. Calculating an average pattern in this way gives more weighting to the high potential time periods, since the normalization was not done before the averaging. The pattern is shown in Figure 6. The basic pattern is a large negative potential cell in the midnight region, with a much smaller positive cell in the afternoon sector.

[39] The CPCP of the patterns were then examined, and a relationship between that and *Dst** was derived. *Dst** tends to peak after the peak in the low-latitude electric field. In addition, the electric field declines much faster than *Dst**. These factors imply that *Dst** may not be the best parameter to fit the CPCP. Figure 7 shows the CPCP of low-latitude

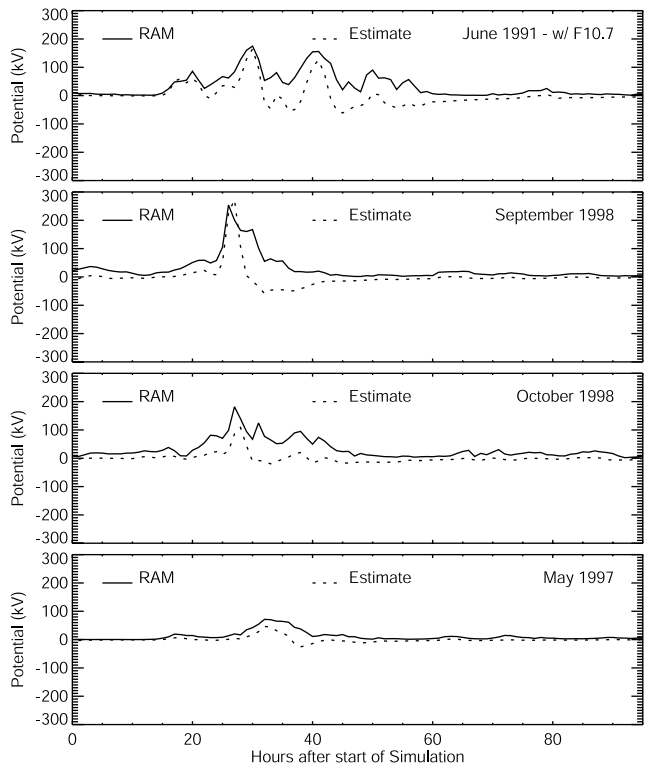

Figure 7. The CPCP and $\alpha \times dD\,st/dt$ for the four storms of interest.

electric potential from all of the storms as well as the time rate of change of the *Dst** multiplied by −16,200. The correlation is very good simply using this proxy. For the June, September, and May storms the peaks occur at the same time and are of similar magnitudes. During the October storm the first peak is well represented, although the magnitude is about half of the actual value. Also, *dDs**/*dt* becomes negative during some time periods, while the potential pattern never reverses in orientation. These differences imply that while the proxy is quite good, there may be better ones. It is interesting to note that the plots are ordered from top to bottom by the *F*10.7 radio flux value, with the top plot being the largest value and the bottom plot being the smallest value. Because the October and May storms underestimate the strength of the CPCP using the simple proxy, the *F*10.7 may be used to correct these underestimates.

[40] Using a linear combination of *Dst** and *dDst**/*dt* with a division by the square root of F10.7, a relationship was derived:

$$\Phi = \left(C_1 Dst^* + C_2 \frac{dDst^*}{dt} \right) \sqrt{\frac{140}{F10.7}}. \quad (3)$$

The two multiplication factors (C_1, in kV nT^{-1}, and C_2, in kV s nT^{-1}) can be adjusted to improve the empirical relationship. In addition, a lower limit of 0 kV and an upper limit of 200 kV were placed on the potential. The adjustment to the parameters was conducted by determining the best fit for different storms (i.e., the ''training storms''), and then the errors were calculated for all of the storms combined. Using this type of method, there is verification that the adjustment parameters work with more storms than they are tested upon.

[41] Table 1 contains a list of training storms, the fitted parameters, and the errors associated with each fit. Each fit was conducted by minimizing the absolute difference between the model-derived potential and the empirical potential for the given storms. The root-mean-square (RMS) error reported in Table is with respect to all of the storms combined. The results show that there is little difference between the different training storms, with only one large exception. Using the September and October storms caused the errors to be much larger than the other runs and caused the correlation to be reduced, because these two storms had high, sharp peaks in the potential. The training methodology forced the other storms to have high, sharp peaks also, which were unrealistic, and therefore caused a large error.

Table 1. Training Run Parameters and Errors

Training Runs	C_1^a	C_2^a	Training Error	RMS Error	Correlation
June, Sept.	−15304	−0.377	13.24	17.64	89.3%
June, Oct.	−16572	−0.377	12.46	17.66	88.8%
June, May	−15567	−0.366	9.44	17.95	89.0%
Sept., Oct.	−28081	−0.372	12.14	20.79	86.4%
Sept., May	−15140	−0.370	9.84	17.86	89.2%
Oct., May	−20670	−0.376	9.37	18.56	87.4%
June, Sept., Oct.	−16143	−0.367	13.00	17.93	88.8%
All	−16763	−0.394	11.41	17.21	89.0%

[a]Constants used in (3).

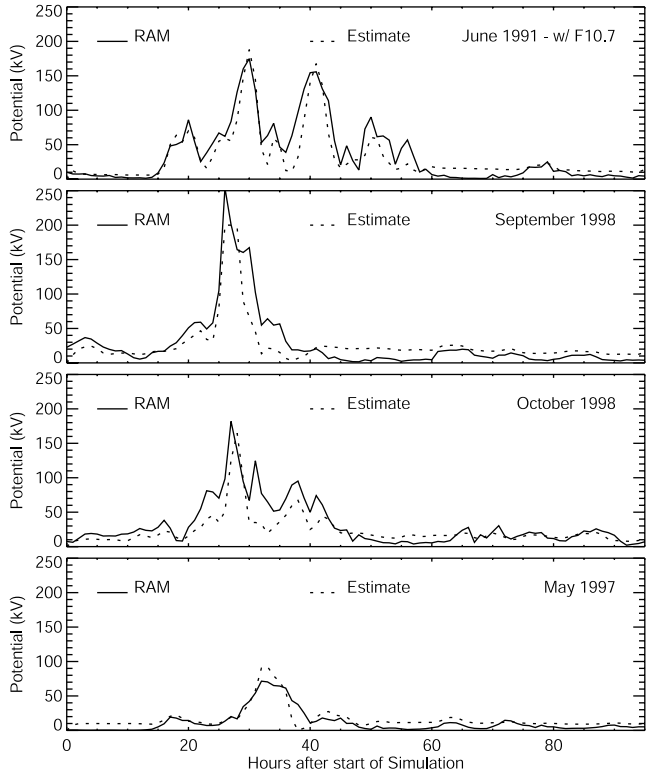

Figure 8. Best representation of a parametric fit to the CPCP using the criteria and formulation discussed in the text. This fit was trained on the June 1991 and October 1998 storms and used the other two storms for validation.

[42] Figure 8 shows the training run on the June 1991 and October 1998 storms, which was an average fit of the storms according to Table. The plots show that the fits are very good. Almost all of the peaks are represented, and the general shape is reproduced. The main difference between the actual and fitted patterns are the widths of the peaks. The peaks in the estimated potentials tend to last less time than the RAM-produced potential peaks and are caused by the use of a linear relationship between the potential and the derivative of *Dst**. Figure 7 shows that this derivative peaks for only a short time. Using a function which elongates these peaks may produce better results but would be much more complicated than the simple linear relationship expressed above.

6. Conclusions

[43] It was found that the storm time ring current is capable of producing an anomalous electric field in the subauroral ionosphere and near-Earth magnetosphere. This electric field is caused by the closure of the asymmetric ring current, which is dominant during the main and early recovery phases of geomagnetic storms and persistent throughout the late recovery phase (although at a much reduced intensity). The presented storm time electric fields are very consistent with observed electric fields in the midlatitude ionosphere and inner magnetosphere. They are also morphologically comparable with asymmetric ring

current generated electric fields from the RCM, which includes the feedback of such fields on the hot ion populations. The results shown above can be considered upper limits to the intensity of this field.

[44] These electric fields will have serious ramifications for space weather, particularly ionospheric scintillation and plasmaspheric reconfigurations (affecting GPS signals, for instance). To parameterize the magnitude of this low-latitude storm time electric field, a relationship has been derived between the CPCP and the *Dst** index. Training of this prediction algorithm on two of the studied storm intervals yields a formulation that accurately reproduces the time sequence of CPCP values for the other two storms. This relation can be used as an initial approximation of the CPCP for inclusion in space weather prediction schemes.

[45] The calculated CPCPs shown in Figure 3 are very large and are sometimes larger than the CPCP of the high-latitude convection pattern (as shown in Figure 4). This implies that ring current models that are run without including a near-Earth electric field are most likely not modeling the deep inner magnetosphere correctly. Because the results discussed here do not include the feedback of this electric field, the field patterns described above will be refined. In particular, it is expected that the inclusion of a self-consistent magnetic field will stretch the pattern to larger radial distances and the inclusion of a self-consistent electric field will deform the pattern in local time (particularly by elongating the negative potential well into the afternoon sector). Because the near-Earth electric field should more rapidly drive plasma through the inner magnetosphere, the magnitude of the low-latitude CPCP will most likely also be reduced by a self-consistent calculation of the asymmetric ring current. All of these corrections to the presented results should bring them more in line with the observed values of low-latitude storm time electric fields. The inclusion of the self-consistent magnetic field and the feedback of the near-Earth electric field are both outside of the scope of the present paper but will be presented in future investigations.

[46] **Acknowledgments.** The RAM calculations require a number of data sets as input and boundary conditions, and regarding this we would like to thank the following: Michelle Thomsen, Joe Borovsky, Fred Rich, Dave McComas, Ron Lepping, and Gang Lu. This work has been supported by NSF grants ATM-0077555 and ATM-0090165 and by NASA grants NAG5-10297, NCC8-181, and NAG-10850.

[47] Janet G. Luhmann thanks Dennis L. Gallagher and another referee for their assistance in evaluating the paper.

References

Belian, R. D., G. R. Gisler, T. Cayton, and R. Christensen, High-Z energetic particles at geosynchronous orbit during the great solar proton event series of October 1989, *J. Geophys. Res.*, *97*, 16,897, 1992.

Burch, J. L., et al., Views of Earth's magnetosphere with the IMAGE satellite, *Science*, *291*, 619, 2001a.

Burch, J. L., D. G. Mitchell, B. R. Sandel, P. Cison Brandt, and M. Wuëst, Global dynamics of the plasmasphere and ring current during magnetic storms, *Geophys. Res. Lett.*, *28*, 1159, 2001b.

Burke, W. J., N. C. Maynard, M. P. Hagan, R. A. Wolf, G. R. Wilson, L. C. Gentile, M. S. Gussenhoven, C. Y. Huang, T. W. Garner, and F. J. Rich, Electrodynamics of the inner magnetosphere observed in the dusk sector by CRESS and DMSP during the magnetic storm of June 4–6, 1991, *J. Geophys. Res.*, *103*, 29,399, 1998.

Cison Brandt, P., D. G. Mitchell, Y. Ebihara, and E. C. Roelof, Understanding the ring current with IMAGE/HENA, *Eos Trans. AGU*, *81*(45), Fall Meet. Suppl., F1036, 2000.

Ebihara, Y., and M. Ejiri, Simulation study on fundamental properties of the storm time ring current, *J. Geophys. Res.*, *105*, 15,843–15,859, 2000.

Fejer, B. G., and L. Scherliess, Empirical models of storm time equatorial zonal electric fields, *J. Geophys. Res.*, *102*, 24,047, 1997.

Fejer, B. G., and L. Scherliess, Mid- and low-latitude prompt-penetration ionospheric zonal plasma drifts, *Geophys. Res. Lett.*, *25*, 3071, 1998.

Fejer, B. G., R. W. Spiro, R. A. Wolf, and J. C. Foster, Latitudinal variation of perturbation electric fields during magnetically disturbed periods: 1986 SUNDIAL observations and model results, *Ann. Geophys.*, *8*, 441, 1990.

Fok, M.-C., Decay of ring current ions and associated aeronomical consequences, Ph.D. thesis, Univ. of Mich., Ann Arbor, 1993.

Fok, M.-C., R. A. Wolf, R. W. Spiro, and T. E. Moore, Comprehensive computational model of the earth's ring current, *J. Geophys. Res.*, *106*, 8417, 2001.

Foster, J. C., and F. J. Rich, Prompt midlatitude electric field effects during severe geomagnetic storms, *J. Geophys. Res.*, *103*, 26,367, 1998.

Foster, J. C., S. Cummer, and U. S. Inan, Midlatitude particle and electric field effects at the onset of the November 1993 geomagnetic storm, *J. Geophys. Res.*, *103*, 26,359, 1998.

Garner, T. W., A case study of the June 4–5 1991 matgnetic storm using the Rice Convection Model, Ph.D. thesis, Rice Univ., Houston, Tex., 2000.

Greenspan, M. E., and D. C. Hamilton, A test of the Dessler-Parker-Sckopke relation during magnetic storms, *J. Geophys. Res.*, *105*, 5419, 2000.

Harel, M., R. A. Wolf, P. H. Reiff, R. W. Spiro, W. J. Burke, F. J. Rich, and M. Smiddy, Quantitative simulation of a magnetosphereic substorm, 1, Model logic and overview, *J. Geophys. Res.*, *86*, 2217, 1981.

Horwitz, J. L., Core plasma in the magnetosphere, *Rev. Geophys.*, *25*, 579, 1987.

Jordanova, V. K., L. M. Kistler, J. U. Kozyra, G. V. Khazanov, and A. F. Nagy, Collisional losses of ring current ions, *J. Geophys. Res.*, *101*, 111, 1996.

Kelley, M. C., *The Earth's Ionosphere*, Academic, San Diego, Calif., 1989.

Kozyra, J. U., M. W. Liemohn, C. R. Clauer, A. J. Ridley, M. F. Thomsen, J. E. Borovsky, J. L. Roeder, and V. K. Jordanova, Multistep *Dst* development and ring current composition changes during the 4–6 June 1991 magnetic storm, *J. Geophys. Res.*, 10.1029/2001JA000023, in press, 2001.

Liemohn, M. W., J. U. Kozyra, C. R. Clauer, and A. J. Ridley, Computational analysis of the near-earth magnetospheric current system, *J. Geophys. Res.*, *107*, 29,531, 10.1029/2001JA000045, 2001a.

Liemohn, M. W., J. U. Kozyra, M. F. Thomsen, J. L. Roeder, G. Lu, J. E. Borovsky, and T. E. Cayton, Dominant role of the asymmetric ring current in producing the storm time *Dst**, *J. Geophys. Res.*, *106*, 10,883, 2001b.

McComas, D. J., S. J. Bame, B. L. Barraclough, J. R. Donart, R. C. Elphic, J. T. Gosling, M. B. Moldwin, K. R. Moore, and M. F. Thomsen, Magnetospheric plasma analyzer: initial three-spacecraft observations from geosynchronous orbit, *J. Geophys. Res.*, *98*, 13,453, 1993.

McIlwain, C. E., A *Kp* dependent equatorial electric field model, *Adv. Space Res.*, *6*(3), 187, 1986.

Moen, J., and A. Brekke, The solar flux influence on quiet-time conductances in the auroral ionosphere, *Geophys. Res. Lett.*, *20*, 971, 1993.

Papitashvili, V. O., F. J. Rich, M. A. Heinemann, and M. R. Hairston, Parameterization of the defense meteorological satellite program ionospheric electrostatic potentials by the interplanetary magnetic field strength and direction, *J. Geophys. Res.*, *104*, 177, 1999.

Reddy, C. A., and H. G. Mayr, Storm time penetration to low latitudes of magnetospheric-ionospheric convection and convection-driven thermospheric winds, *Geophys. Res. Lett.*, *25*, 3075, 1998.

Ridley, A. J., G. Crowley, and C. Freitas, An empirical model of the ionospheric electric potential, *Geophys. Res. Lett.*, *27*, 3675, 2000.

Roble, R. G., and E. C. Ridley, An auroral model for the NCAR thermospheric general circulation model (TGCM), *Ann. Geophys., Ser. A*, *5*, 369, 1987.

Rowland, D. E., and J. R. Wygant, Dependence of the large-scale, inner magnetospheric electric field on geomagnetic activity, *J. Geophys. Res.*, *103*, 14,959, 1998.

Ruohoniemi, J. M., and R. A. Greenwald, Statistical patterns of the high-latitude convection obtained from Goose Bay HF radar observations, *J. Geophys. Res.*, *101*, 21,753, 1996.

Southwood, D. J., and R. A. Wolf, An assessment of the role of precipitation in magnetospheric convection, *J. Geophys. Res.*, *83*, 5227, 1978.

Spiro, R. W., and R. A. Wolf, Electrodynamics of convection in the inner magnetosphere, in *Magnetospheric Currents, Geophys. Monogr. Ser.*, vol. 28, edited by T. A. Potemra, p. 247, AGU, Washington, D. C., 1984.

Spiro, R. W., R. A. Wolf, and B. G. Fejer, Penetration of high-latitude-electric-field effects to low latitudes during SUNDIAL 1984, *Ann. Geophys.*, *6*, 39, 1988.

Stern, D. P., The motion of a proton in the equatorial magnetosphere, *J. Geophys. Res.*, *80*, 595, 1975.

Takahashi, S., M. Takeda, and Y. Yamada, A simulation of the storm-time partial ring current system and the dawn-dusk asymmetry of geomagnetic variation, *Planet. Space Sci.*, *39*, 821, 1991.

Volland, H., A semiempirical model of large-scale magnetospheric electric fields, *J. Geophys. Res.*, *78*, 171, 1973.

Weimer, D. R., A flexible, IMF dependent model of high-latitude electric potential having "space weather" applications, *Geophys. Res. Lett.*, *23*, 2549, 1996.

Wygant, J., D. Rowland, H. J. Singer, M. Temerin, F. Mozer, and M. K. Hudson, Experimental evidence on the role of the large spatial scale electric field in creating the ring current, *J. Geophys. Res.*, *103*, 29,527, 1998.

Yeh, H.-C., J. C. Foster, F. J. Rich, and W. Swider, Storm time electric field penetration observed at midlatitude, *J. Geophys. Res.*, *96*, 5707, 1991.

Young, D. T., H. Balsiger, and J. Geiss, Correlations of magnetospheric ion composition with geomagnetic and solar activity, *J. Geophys. Res.*, *87*, 9077, 1982.

M. W. Liemohn and A. J. Ridley, Space Physics Research Laboratory, University of Michigan, Ann Arbor, Michigan, 49109-2143, USA. (liemohn@umich.edu; ridley@umich.edu)